Before operating on the matrix $[A]^{-1}$, the $\mathbf{r}_n$ vector (in the **ijk** system), which defines the positions of the $n$th structural unit, should be added to the $(x_T y_T z_T)$ $[T]$ vector. So that the final formula is

$$(x_{PF}y_{PF}z_{PF}) = \{(x_T y_T z_T)\,[T] + (r_{nx}r_{ny}r_{nz})\}\,[A]^{-1}.$$

### References


ANDERSSON, S. (1978). *J. Solid State Chem.* **23**, 191–204.
FRANK, F. C. & KASPER, J. S. (1958). *Acta Cryst.* **11**, 184–196.
FRANK, F. C. & KASPER, J. S. (1959). *Acta Cryst.* **12**, 483–499.
HIRAGA, K., YAMAMOTO, T. & HIRABAYASHI, M. (1983). *Trans. Jpn Inst. Met.* **24**, 421–430.
ISHIZUKA, K. (1982). *Acta Cryst.* A**38**, 773–779.
KOMURA, Y., TAKEDA, S. & TAKATA, M. (1983). *Trans. Jpn Inst. Met.* **24**, 315–322.
KUO, K. H., YE, H. Q. & LI, D. X. (1986). *J. Mater. Sci.* **21**, 2597–2622.
LI, D. X. & KUO, K. H. (1986). *Acta Cryst.* B**42**, 152–159.
PEARSON, W. B. (1972). *The Crystal Chemistry and Physics of Metals and Alloys.* New York: Wiley–Interscience.
SHOEMAKER, D. P. & SHOEMAKER, C. B. (1969). *Developments in the Structural Chemistry of Alloy Phases*, pp. 107–139. New York: Plenum.
SHOEMAKER, D. P. & SHOEMAKER, C. B. (1972). *Acta Cryst.* B**28**, 2957–2965.
SHOEMAKER, D. P. & SHOEMAKER, C. B. (1986). *Acta Cryst.* B**42**, 3–18.
WANG, D. N., YE, H. Q. & KUO, K. H. (1986). *Acta Cryst.* B**42**, 21–25.
YE, H. Q. (1987). *J. Electron Microsc. Tech.* **7**, 283–292.
YE, H. Q., LI, D. X. & KUO, K. H. (1984). *Acta Cryst.* B**40**, 461–465.
YE, H. Q., LI, D. X. & KUO, K. H. (1985). *Philos. Mag.* **51**, 829–837.
YE, H. Q., WANG, D. N. & KUO, K. H. (1985). *Philos. Mag.* **51**, 839–848.


*Acta Cryst.* (1989). B**45**, 6–13

# Grain Boundary Structure Analysed by a Coincidence-Site-Lattice Pattern for a Layer Stacking Structure of the 4*H*-Type Laves Phase

BY M. TAKATA, Y. KITANO AND Y. KOMURA

*Department of Materials Science, Faculty of Science, Hiroshima University, Higashi-senda-machi, Naka-ku, Hiroshima* 730, *Japan*

(*Received* 15 *May* 1987; *accepted* 20 *July* 1988)


## Abstract

A coincidence-site-lattice (CSL) model is applied to the 4*H*-type layer stacking structure of $Mg(Cu,Al)_2$ alloys of the Laves phase, in order to analyse the structure of densely packed plane (DPP) boundaries which are observed by high-resolution electron microscopy (HREM). In this analysis 'lattice point' is used in a wide sense, including all the origins of the repeating unit in every layer. Owing to this extension, extra coincidence sites of lattice points (CSL-points) occur in the interpenetrating lattices and produce a characteristic pattern which is called a CSL-pattern in this paper. The CSL-pattern gives a satisfactory model for the boundary structure of layer stacking structures such as the Laves phase. Basis vectors of the displacement-shift-complete (DSC) lattice obtained here are smaller than those of the usual DSC-lattice and explain well the Burgers vectors of grain boundary dislocations (GBD's). Step vectors and step heights associated with the GBD's are also discussed in detail for the DPP-boundary.


## 1. Introduction

It has been verified by HREM that the CSL-model is useful for investigations of repeating structures of grain boundaries (Ichinose & Ishida, 1981; d'Anterroches & Bourret, 1984). Since most layer stacking structures have unit cells of considerable size in the stacking direction, CSL-points are sparse in interpenetrating lattices and give limited information about the periodicity of the boundary structure with a long period. In order to obtain more information from interpenetrating lattices, we adopt all the origins of the repeating unit in every layer as 'lattice points' when drawing the interpenetrating lattices. This extension of 'lattice point' is applied to the 4*H* structure of the Laves phase to analyse the boundary structure.

The Laves phase is one of the intermetallic compounds having tetrahedrally close-packed structures. But the crystal structure of the Laves phase is simply understood to be a layer stacking structure of basal planes (Komura, 1962), where one layer is composed of four densely packed atomic planes and is called a fundamental layer of the Laves phase. For example, three basic structures of the Laves phase, $MgZn_2$-(*C*14)-type (Friauf, 1927*a*), $MgCu_2$(*C*15)-type (Friauf, 1927*b*) and $MgNi_2$(*C*36)-type (Laves & Witte, 1935), are illustrated in Fig. 1, where each drawing is divided into two, three or four fundamental layers by dotted lines. In a unit cell of the *C*14 structure two fundamental layers stack similar to the h.c.p. layer sequence,

0108-7681/89/010006-08$03.00

so this structure is called $2H$. In $C15$ and $C36$, the fundamental layers stack similar to the f.c.c. and d.h.c.p. layer sequences so these are called $3C$ and $4H$, respectively. Since the fundamental layers have almost the same atomic configuration except for relative shifts in basal plane, all the origins in the fundamental layers are adopted as lattice points in deriving a CSL.

Recently, linear defects at the interfaces between two different stacking variants and several types of dislocations in $Mg(Cu,Zn)_2$ were investigated by HREM (Kitano, Komura, Kajiwara & Watanabe, 1980; Takeda, Kitano & Komura, 1983; Kitano, Takata & Komura, 1986). Some symmetric grain boundaries were also observed in the same system and it was found that the rotation angle between two adjoining crystals depends upon the type of stacking variants (M. Takata, Y. Kitano, S. Takeda & Y. Komura, in preparation). In an alloy system of $Mg(Cu,Al)_2$, tilt boundaries having a rotation of 70·5° around [110] of the hexagonal cell, which is denoted by 70·5°/[110], are frequently found. The angle 70·5° is equal to the angle between two faces of a tetrahedron formed by small atoms in the Laves-phase structure. From HREM observation, boundaries are found to be parallel to the basal plane of one of two crystals. Therefore, these will be called densely packed plane (DPP) boundaries in this paper.

For extended CSL-models, an elegant method has been developed on the basis of group theory by Pond & Bollmann (1979) and Pond & Vlachavas (1983). In the present article an example which is more geometrically intuitive and more practical will be demonstrated.

In this study, the CSL-model based on the extension of the meaning of the lattice point is applied to the DPP-boundary of the $4H$ layer stacking structure. This extension gives a characteristic pattern of CSL-points which enables us to investigate a detailed structure at the boundary. In addition, the present analysis predicts a new type of Burgers vector for a GBD. Similar boundaries between two crystallites of $2H$ structure as well as between two different layer stacking structures were discussed in separate papers (Takata, Kitano & Komura, 1986; Kitano, Takata & Komura, 1989).

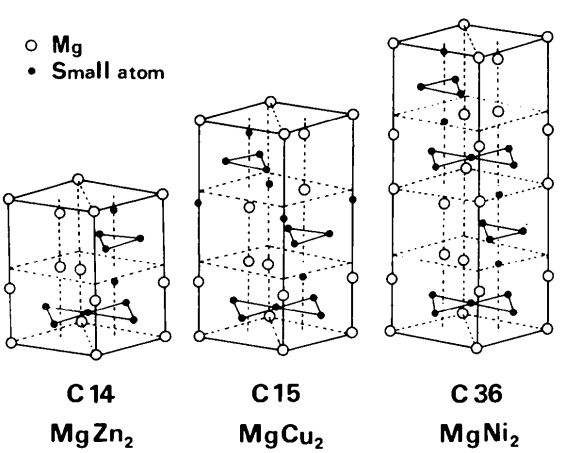


Fig. 1. Three basic structures of the Laves phase. Open circles: Mg atoms; full circles: smaller atoms (Zn, Cu or Ni). Unit cells are divided into two, three and four fundamental layers by dotted lines for $MgZn_2$, $MgCu_2$ and $MgNi_2$ structures, respectively.

## 2. Experimental procedure

Alloy specimens $Mg(Cu_{1-x}Al_x)_2$ with $x = 0{\cdot}465$ were prepared by melting suitable amounts of pure Mg and mother alloys of Cu–Al together with an appropriate amount of Cu in an argon-filled induction furnace. The metals used here were 99·9% grade. The melt was vigorously stirred and cast into a cylindrical graphite mold. Ingots were sliced into discs 0·2 mm thick, and the discs were electrolytically polished in a mixture of $HNO_3$ and $CH_3OH$. Finally Ar-ion thinning was employed. The specimens were examined under a JEM 200CS electron microscope operated at 200 kV. With a double-tilting goniometer of a side-entry type, the [110] direction was set exactly parallel to the incident beam. The coefficients of the spherical and chromatic aberration of the objective lens were both 1·9 mm. Images were taken after inserting an objective aperture of radius 1/2·5 $Å^{-1}$ at the centre of the $h\bar{h}l$ net plane.

## 3. Crystal structure and image contrast of the $4H$ Laves phase

As is shown in Fig. 1, the crystal structure of the $4H$ Laves phase ($C36$ type) is described as an ...$ABAC$... layer sequence which is represented similarly to the d.h.c.p. structure. The crystal structure was originally analysed by Laves & Witte (1935), and details of the atomic arrangements have been discussed in connection with a stacking fault (Komura, 1962; Kitano, Takata & Komura, 1986). HREM work on the Laves phase has been performed by Kitano, Komura, Kajiwara & Watanabe (1980) and a correspondence between image contrast and crystal structure has been discovered.

A structure image of the $4H$ structure projected in the [110] direction is presented in Fig. 2. A projection of the structure is inserted in the structure image. In this projection, large open circles correspond to columns of Mg atoms, and small open circles and dots to columns of Al or Cu atoms. Atoms connected by full lines lie on one plane and atoms connected by dotted lines on the other. These two types of planes are alternately stacked in the projection direction with dotted atoms placed in between. So, the density of atoms of a dot inside a pentagon is twice that of small or large open circles.

From the HREM image of Fig. 2 it is easily recognized that the rows of bright dots along the $[\bar{1}10]$ direction stack in the **c** direction with a shift of $\frac{1}{3}[\bar{1}10]$ or $-\frac{1}{3}[\bar{1}10]$ in the same way as the stacking sequence

...*ABAC*... of the d.h.c.p. structure. Therefore, it is concluded that only the 'lattice points' in the wide sense which is used throughout this paper are visible in the structure image.

It is confirmed by image calculations of the multislice method that a bright dot in the structure image corresponds to an atomic column with the highest density which is indicated by dots in the projection (Takeda, Kitano & Komura, 1983). The structure image, the projection of the crystal structure and the calculated image contrast are compared in Fig. 2. The calculated image is obtained for a crystal thickness of 100 Å, and for a defocus value of −800 Å which is nearly equal to the optimum defocus value. It is verified that the correspondence between image contrast and crystal structure is maintained over wide ranges of defocus and crystal thickness. The stacking sequence is easily coded from the structure images. The calculation was carried out by a computer program for the multislice method produced by Takeda (1983).

## 4. CSL-points and CSL-pattern

As mentioned above, the crystal structure of the Laves phase is described as a layer structure. In drawing interpenetrating lattices we will take all the origins in every layer as 'lattice points'. The interpenetrating lattices related by a 70·5° rotation about [110] are given in Fig. 3. In Figs. 3 and 4 (discussed below) filled circles and open circles represent 'lattice points' of crystal I and crystal II, respectively, and circles with a dot represent CSL-points. The size of the circles represents a difference in atomic position perpendicular to the plane of the figure: lattice points in the plane of the figure are shown by large circles but those above or below by small circles.

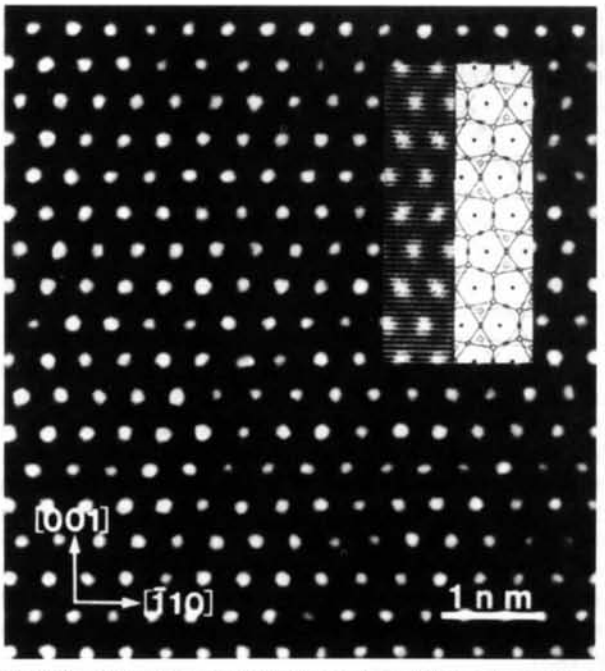


Fig. 2. Structure image of the 4*H* Laves phase (*C*36) projected along [110]. A projection of the structure and a calculated image contrast are inserted. The rows of the bright dots along the [$\bar{1}$10] direction stack in the **c** direction in the same way as for the d.h.c.p. structure. [1 nm ≡ 10 Å.]

In Fig. 3, projections of the unit cells of two 4*H* crystals are given by rectangles. Eight 'lattice points' are included in each rectangle. The rhombus *RSTU* of dotted lines in Fig. 3 is a periodic unit in the interpenetrating lattices and has the same size as that of the CSL usually used. As easily seen in Fig. 3, sixteen CSL-points in the rhombus *RSTU* are found and they show a characteristic pattern which is called a CSL-pattern in this paper. The size of the rhombus would predict the periodicity of the boundary structure and the CSL-pattern would give detailed information within one period. The CSL-pattern varies with respect to the stacking sequence of the layer structure.

The lattice parameters of a hexagonal cell for the 4*H*-type $Mg(Cu,Al)_2$ Laves phase are $a_o \equiv |\mathbf{a}| = 5{\cdot}11$ Å and $c_o \equiv |\mathbf{c}|/4 = 4{\cdot}17$ Å (Komura, 1962). Thus, the axial ratio, $c_o/a_o$, becomes equal to a particular value, $\sqrt{(8/3)}/2 = 0{\cdot}816$, which is half the axial ratio of the ideal h.c.p. structure. In drawing the CSL-pattern we use this ideal value.

## 5. DSC-lattice for the 4*H*-type layer structure

A DSC-lattice is defined as the coarsest lattice which contains both crystal lattices as sublattices (Bollmann, 1970). The DSC-lattice in the plane of Fig. 3 is shown in Fig. 4. From this drawing it is found that the basis vectors of the DSC-lattice are

$$\mathbf{b}_1 = (-4\mathbf{a} + 4\mathbf{b} + 3\mathbf{c})/36 = [\bar{4}43]/36 = [\bar{1}1\tfrac{3}{4}]/9 \quad (1)$$

$$\mathbf{b}_2 = (8\mathbf{a} - 8\mathbf{b} + 3\mathbf{c})/36 = [8\bar{8}3]/36 = [2\bar{2}\tfrac{3}{4}]/9, \quad (2)$$

referring to crystal I whose lattice is represented by filled circles. Here **a**, **b** and **c** are the unit-cell vectors of the hexagonal cell of the 4*H* structure. The vectors $\mathbf{b}_1$ and $\mathbf{b}_2$ are equal to the basis vectors of the DSC-lattice for the 2*H* structure (Takata *et al.*, 1986). The reason why these vectors are equal to each other is as follows: Since each fundamental layer stacks in the **c** direction with a shift of $[\bar{1}10]/3$ or $-[\bar{1}10]/3$, the translation vector $\mathbf{t}_1$ or $\mathbf{t}_2$ between two successive layers is represented by:

$$\mathbf{t}_1 = \tfrac{1}{3}[\bar{1}10] + \tfrac{1}{4}[001] = \tfrac{1}{3}[\bar{1}1\tfrac{3}{4}]$$

or

$$\mathbf{t}_2 = \tfrac{1}{3}[1\bar{1}0] + \tfrac{1}{4}[001] = \tfrac{1}{3}[1\bar{1}\tfrac{3}{4}].$$

From equations (1) and (2) these equations may be rewritten

$$\mathbf{t}_1 = 3\mathbf{b}_1 \quad (3)$$

$$\mathbf{t}_2 = \mathbf{b}_1 + 2\mathbf{b}_2. \quad (4)$$

It is concluded that the vectors $\mathbf{t}_1$ and $\mathbf{t}_2$ which are the possible translation vectors from one layer to the next are represented by linear combinations of the DSC-lattice vectors $\mathbf{b}_1$ and $\mathbf{b}_2$. Since any type of regular structure or any type of stacking faulted structure is represented by a sequence of translation vectors, $\mathbf{t}_1$ or $\mathbf{t}_2$, all the lattice points can be represented by a linear combination of $\mathbf{b}_1$ and $\mathbf{b}_2$. From the definition of the DSC-lattice the vectors $\mathbf{b}_1$ and $\mathbf{b}_2$ would be the basis vectors even if any stacking variants were considered or any changes in stacking sequence occurred in a regular structure.

## 6. Experimental results

By HREM observation, 70·5°/[110] boundaries are found from place to place in this alloy. A parameter $\Sigma$ which refers to a reciprocal density of coincidence lattice points is equal to $\Sigma 9$. This value is the minimum among the boundaries generated by rotation about the

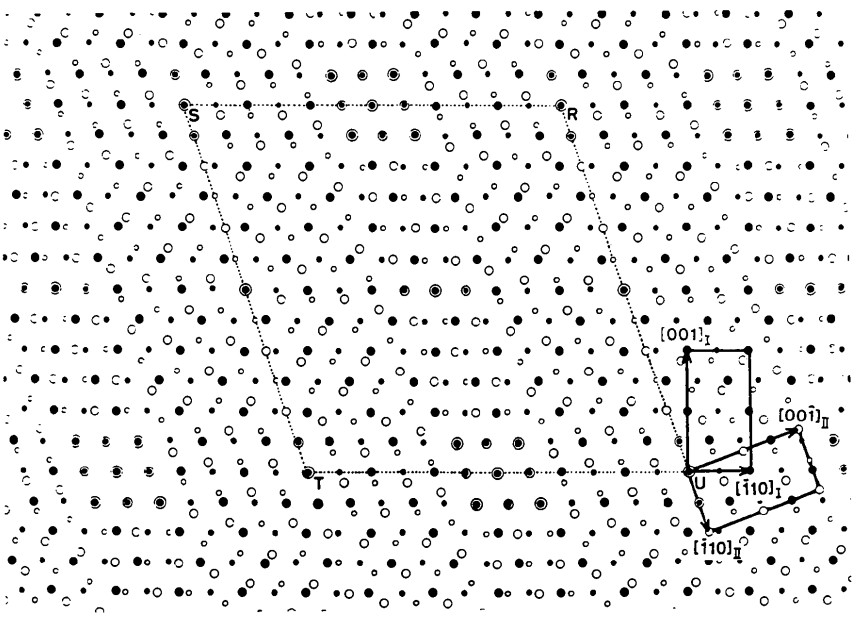


Fig. 3. Interpenetrating lattices for two $4H$ layer structures with a 70·5° rotation about [110]. All the origins of the repeat unit in every layer are adopted as 'lattice points'. Projections of the unit cells of two $4H$ crystals are shown by rectangles. Filled circles belong to crystal I, open circles to crystal II. Circles with a dot represent the CSL-points. A characteristic pattern of the CSL-points is obtained and is called a CSL-pattern. The rhombus $RSTU$ represents a unit cell in the interpenetrating lattices and the vectors **TS** and **TU** are the basis vectors of the CSL.

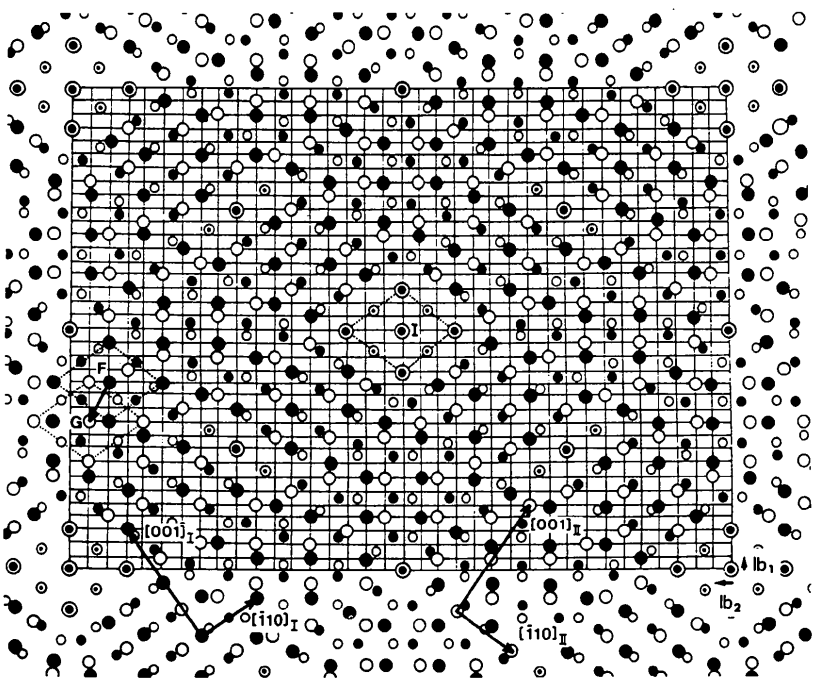


Fig. 4. The DSC-lattice derived from the interpenetrating lattices of Fig. 3. The vectors $\mathbf{b}_1$ and $\mathbf{b}_2$ are basis vectors of the DSC-lattice. The vector **FG** is equal to $-3\mathbf{b}_1 + \mathbf{b}_2$.

[110] axis. Boundary planes are frequently found to be parallel to the DPP (*i.e.* basal planes) of one of the component crystals. In this paper, a crystal whose basal plane is parallel to the boundary is named crystal I and the other crystal II. One of the lattice images of the DPP-boundary of $\Sigma 9$ in the 4*H* structure is shown in Fig. 5. In this image, the boundary is parallel to the (001) DPP of crystal I and the rotation angle of the two crystals is 70·5°. A characteristic repetition is observed along the boundary. But the periodicity is broken at a boundary step *C* at the centre of the image. A stacking fault (SF) shown by a horizontal arrow terminates at the boundary step *C*.

Except for the boundary step *C* the boundary is made up of a continuous alternation of clear and disturbed regions of the structure image. In the clear regions the $[\bar{1}10]$ arrays of bright dots of crystal II connect smoothly with bright dots of crystal I, but in the disturbed regions images are vague between the two crystals. We call the former region a boundary bridge, and the latter a perturbed region.

Fundamental layers in crystal II which reach boundary bridges are indicated by arrows parallel to the $[\bar{1}10]_{II}$ direction towards the top of Fig. 5 (similarly in Figs. 6 and 7 discussed below). A boundary structure is represented by a series of numerals which indicate the numbers of the fundamental layers in crystal II alternately belonging to the bridges and the perturbed regions. For example, in Fig. 5 the boundary structure is described from left to right as ...[4]1[4]3[5]3-[4]1[4]3[4]1[4]3..., where numerals in brackets show the numbers of the fundamental layers in crystal II which meet the perturbed region at the boundary and numerals not in brackets show the numbers of the fundamental layers in crystal II which reach the boundary bridge. The periodic unit of the boundary structure is found to be [4]1[4]3, but a sequence [5]3 is inserted around the boundary step *C*, which will be discussed later in detail.

## 7. Discussion

In this section we will use the CSL-pattern proposed in §4 to analyse the results of the HREM observation. It is reasonably assumed that boundaries have a tendency to pass through as many CSL-points as possible.

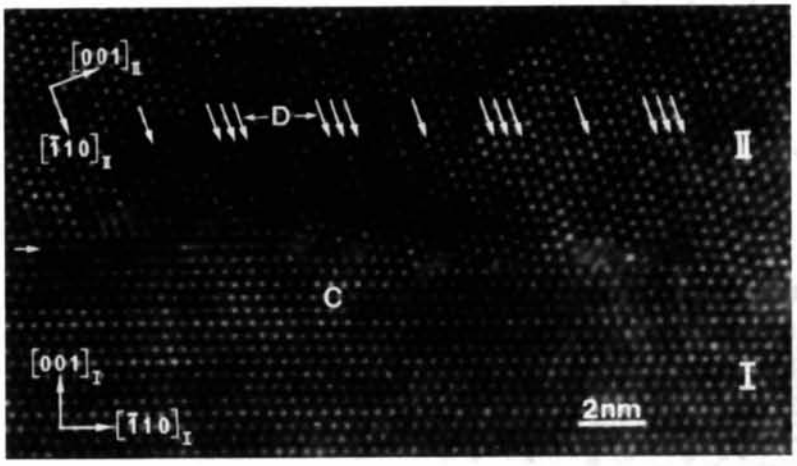


Fig. 5. Structure image of the DPP-boundary in the 4*H* structure. A boundary step *C* is seen at the centre of photograph. An SF indicated by an arrow at the left side of the micrograph terminates at the step. [1 nm ≡ 10 Å.]

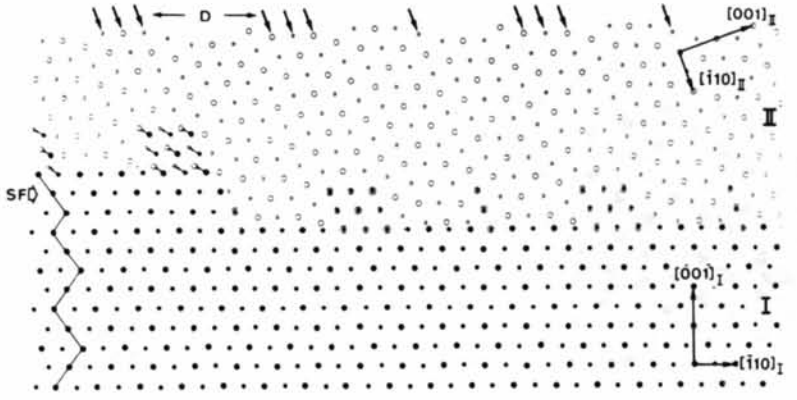


Fig. 6. Primitive boundary model based on Fig. 3. The stacking sequence of crystal I is represented by a zigzag line and an SF is seen at the left side of the step.

### 7.1. *Model of atomic configuration at the boundary*

The structure image of the tilt boundary shown in Fig. 5 is recognized to possess the characteristic feature of the CSL-pattern given in Fig. 3. Since the bright dots in the image correspond to the 'lattice points' as described above, we can first propose a primitive boundary model which is shown in Fig. 6, where we only draw 'lattice points'. As indicated by a dotted line in the figure, the boundary passes through clusters of the CSL-points along the shortest path. This suggests that not only the periodicity but also the detailed structure within a period can be predicted from the CSL-pattern. Clusters of the CSL-points regularly appear and repeat every twelve layers of crystal II as seen in Fig. 6. To interpret the structure image of Fig. 5 the alternating appearance of clear and perturbed areas at the boundary should be compared with the proposed model of Fig. 6.

The atomic configuration at the boundary is constructed using the correspondence between the structure image and the crystal structure explained in Fig. 2. The result is shown in Fig. 7. It is reasonable to assume that in the boundary bridge the atomic configuration is not affected so much and almost all the atomic sites are shared between the two crystals. The associated rigid-body translation should then be equal to zero. On the other hand, the atomic configuration in the perturbed areas cannot be deduced from the structure image or the CSL-pattern. Thus, no atoms are drawn in the perturbed areas in Fig. 7.

### 7.2. *DSC-dislocation due to a boundary step with a stacking fault (SF)*

As described before, a boundary step is seen at the centre indicated by $C$ in Fig. 5. The boundary step occurs at a terminal of an SF in crystal I and the height of the step is found to be equal to a thickness of three fundamental layers, $3c_0 \equiv 3|\mathbf{c}|/4 = 12{\cdot}51$ Å, and the periodicity in the boundary structure is broken.

The boundary structure around $C$ is represented by the series ...[4]1[4]3[$\underline{5}$]3[4]1... instead of the regular series [4]1[4]3. The irregular part [5]3 consists of eight layers of crystal II and is indicated by $D$ and the neighbouring three arrows in Figs. 5 and 6. From the structure image it is known that due to the step the periodic boundary structure shifts along the boundary by $-(4+\frac{1}{3})[\bar{1}10] + \frac{3}{4}[001]$ of crystal I, where the former component $-(4+\frac{1}{3})[\bar{1}10]$ corresponds to [5]3 and the latter $\frac{3}{4}[001]$ to the step height. Except for this area the boundary structure [4]1[4]3 remains unchanged on the left and right sides of the boundary step $C$. If a model of strain-free crystals were drawn beyond the step referring to the right side of structure image, a gap would appear between two crystals in the left area. This situation is shown in two dotted lines in Fig. 6.

This suggests the existence of a GBD, a Burgers vector of which is indicated by the arrows near the gap in Fig. 6. The Burgers vector is equal to $\mathbf{b}_2$ which is predicted from the DSC-lattice based on the CSL-pattern presented in the previous section. Without the extension of the meaning of the lattice point, this type of Burgers vector would not be predicted for a GBD. In an HREM image of the $2H$ structure, a GBD has also been found at a step, and the Burgers vector is shown to be $\mathbf{b}_1$ by the same method (Takata, Kitano & Komura, 1986). Therefore, we conclude that the GBD's observed here are so-called DSC-dislocations.

### 7.3. *Step height of densely packed plane (DPP) boundaries*

A method for the determination of the boundary step height by construction has been given by King & Smith (1980), and it has been shown that a convenient parameter associated with a GBD is a step vector $\mathbf{s}$, which is defined as a shift in the CSL-pattern caused by the passage of a GBD. It is the purpose of this section to derive formulae for the step vector as a function of a Burgers vector of a GBD, and to apply these formulae to the calculation of a boundary step height accompanied by an SF. The formulae of the step vectors for the $2H$ structure are also given in this section.

Part of the DSC-lattice of Fig. 4 is magnified and shown in Fig. 8. In this figure, filled circles belong to crystal I and open ones to crystal II. In the case of $\Sigma 9$ ($70{\cdot}5°/[110]$), the basis vectors $\mathbf{b}_1$ and $\mathbf{b}_2$ of the DSC-lattice are given by equations (1) and (2), respectively. If it is supposed that crystal II is kept stationary while crystal I is displaced by $\mathbf{b}_1$ or $\mathbf{b}_2$, a step vector $\mathbf{s}(\mathbf{b}_1)$ or $\mathbf{s}(\mathbf{b}_2)$ is defined as the shortest vector that joins an 'old' CSL-point to a 'new' one; *i.e.* it runs from

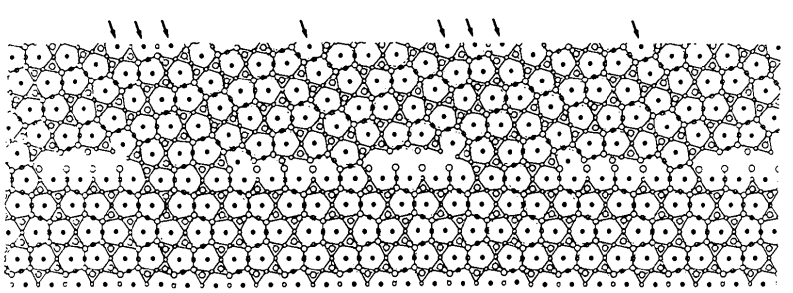

Fig. 7. Model of the atomic configuration on the DPP-boundary in the $4H$ structure.

a lattice point which was coincident before displacement to one which is coincident after it. The reference lattice for all the vectors used hereafter will be the crystal lattice of crystal I.

The primitive step vectors $\mathbf{s}(\mathbf{b}_1)$ and $\mathbf{s}(\mathbf{b}_2)$ are shown in Fig. 8 and are given in Table 1 for the 4*H* structure. In Table 1 all the vectors are written in two different ways; one is represented by the basis vectors $\mathbf{b}_1$, $\mathbf{b}_2$, of the DSC-lattice and the other by the crystallographic vectors of crystal I. In the latter case, three orthogonal vectors [110], [$\bar{1}$10], [001] of the hexagonal system are used. The direction [110] is perpendicular to the plane of the micrograph of the HREM image and is parallel to the rotation axis of the two crystals. Both axes [$\bar{1}$10] and [001] lie in the plane of the micrograph. The fundamental layer of crystal I is parallel to [$\bar{1}$10] and is perpendicular to [001]. The CSL-vectors in Table 1 are defined as the translation vectors of the CSL which are equal to the vectors **TS** and **TU** in Fig. 3. In Table 1 $\mathbf{Z}_{CSL}$ is the third basis vector of the CSL and has a component along the rotation axis [110], *i.e.* $\mathbf{Z}_{CSL}$ is perpendicular to the plane of Fig. 8. As is shown in Table 1, the primitive step vector $\mathbf{s}(\mathbf{b}_1)$ or $\mathbf{s}(\mathbf{b}_2)$ possesses a [110] component and is equal to $\frac{1}{2}$[110].

Supposing a GBD with a Burgers vector $m\mathbf{b}_1 + n\mathbf{b}_2$ ($m$, $n$ are integers) passes through the boundary or any type of such displacement occurs in crystal I, a shift of the CSL-pattern represented by $\mathbf{s}(m\mathbf{b}_1 + n\mathbf{b}_2)$ occurs. From the linearity of the step vector, $\mathbf{s}(m\mathbf{b}_1 + n\mathbf{b}_2)$ is divided into the two following terms:

$$\mathbf{s}(m\mathbf{b}_1 + n\mathbf{b}_2) = m\mathbf{s}(\mathbf{b}_1) + n\mathbf{s}(\mathbf{b}_2). \tag{5}$$

Using the equations in Table 1, we obtain

$$\begin{aligned}\mathbf{s}(m\mathbf{b}_1 + n\mathbf{b}_2) &= \tfrac{5}{2}m[\bar{1}10] - m[001] + \tfrac{3}{2}n[\bar{1}10] + n[001] \\ &\quad + \tfrac{1}{2}(m+n)[110] \\ &= (\tfrac{5}{2}m + \tfrac{3}{2}n)[\bar{1}10] + (-m+n)[001] \\ &\quad + \tfrac{1}{2}(m+n)[110]. \end{aligned} \tag{6}$$

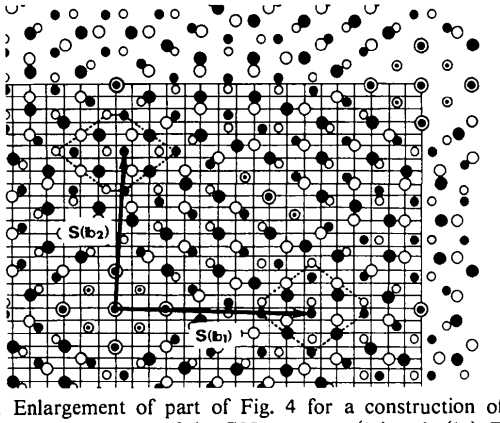


Fig. 8. Enlargement of part of Fig. 4 for a construction of the primitive step vectors of the CSL-pattern, $\mathbf{s}(\mathbf{b}_1)$ and $\mathbf{s}(\mathbf{b}_2)$. These steps are caused by the passage of GBD's with Burgers vectors $\mathbf{b}_1$ and $\mathbf{b}_2$.

Table 1. *Basis vectors of the DSC-lattice and of the CSL, and step vectors of the CSL-pattern for the 4H and 2H structures* ($\Sigma$9, 70·5°/[110])

| 4*H* structure | 2*H* structure |
|---|---|
| DSC-vectors | |
| $\mathbf{b}_1 = \frac{1}{9}[\bar{1}1\frac{3}{4}]$ | $\mathbf{b}_1 = \frac{1}{9}[\bar{1}1\frac{3}{2}]_{2H}$ |
| $\mathbf{b}_2 = \frac{1}{9}[22\frac{3}{4}]$ | $\mathbf{b}_2 = \frac{1}{9}[22\frac{3}{2}]_{2H}$ |
| CSL-vectors | |
| $\mathbf{TS} = 18(\mathbf{b}_1 + \mathbf{b}_2)$ | $\mathbf{TS} = 9(\mathbf{b}_1 + \mathbf{b}_2)$ |
| $= -2[\bar{1}10] + 3[001]$ | $= -[\bar{1}10] + 3[001]_{2H}$ |
| $\mathbf{TU} = 18(\mathbf{b}_1 - \mathbf{b}_2)$ | $\mathbf{TU} = 9(\mathbf{b}_1 - \mathbf{b}_2)$ |
| $= 6[\bar{1}10]$ | $= 3[\bar{1}10]$ |
| $\mathbf{Z}_{CSL} = [110]$ | $\mathbf{Z}_{CSL} = [110]$ |
| Step vectors of the CSL-pattern | |
| $s(\mathbf{b}_1) = -\frac{1}{4}(23\mathbf{b}_2 + \mathbf{b}_1) + \frac{1}{2}\mathbf{z}_{CSL}$ | $s(\mathbf{b}_1) = \frac{1}{2}(13\mathbf{b}_2 - \mathbf{b}_1) + \frac{1}{2}\mathbf{z}_{CSL}$ |
| $= \frac{3}{4}[\bar{1}10] - [001] + \frac{1}{2}[110]$ | $= -\frac{3}{2}[\bar{1}10] + [001]_{2H} + \frac{1}{2}[110]$ |
| $\mathbf{s}(\mathbf{b}_2) = \frac{1}{4}(25\mathbf{b}_1 - \mathbf{b}_2) + \frac{1}{2}\mathbf{z}_{CSL}$ | $\mathbf{s}(\mathbf{b}_2) = -\frac{1}{2}(11\mathbf{b}_1 + \mathbf{b}_2) + \frac{1}{2}\mathbf{z}_{CSL}$ |
| $= \frac{3}{2}[\bar{1}10] + [001] + \frac{1}{2}[110]$ | $= -\frac{1}{2}[\bar{1}10] - [001]_{2H} + \frac{1}{2}[110]$ |

The first term of the right-hand side is related to a shift of the boundary structure along the boundary plane, and the second is related to the boundary step height. In this case, the third term is of no importance, because an identical CSL-pattern is recreated by this displacement. So we hereafter ignore the third term. In this way we can determine the shift of the periodic boundary structure along the DPP-boundary as well as the boundary step height. In order to obtain the real step vectors in crystal I, the basis vectors of the CSL (Table 1) must be added to or subtracted from equation (6).

The boundary step at *C* in Fig. 5 is caused by an SF together with a GBD. A displacement of crystal I due to the SF is found to be $-\mathbf{t}_1 = -3\mathbf{b}_1$ [equation (3)] from the HREM image. As shown in Fig. 6 the Burgers vector of the GBD is $\mathbf{b}_2$. Therefore, the total displacement vector of crystal I is $-3\mathbf{b}_1 + \mathbf{b}_2$ relative to crystal II. Substituting this vector into equation (6) we obtain the total step vector to be

$$\begin{aligned}\mathbf{s}(-3\mathbf{b}_1 + \mathbf{b}_2) &= -3\mathbf{s}(\mathbf{b}_1) + \mathbf{s}(\mathbf{b}_2) \\ &= -6[\bar{1}10] + 4[001] \\ &= -4[\bar{1}10] + [001] + \{-2[\bar{1}10] \\ &\quad + 3[001]\}. \end{aligned} \tag{7}$$

If we subtract a basis vector (**TS** in Fig. 3) of the CSL which is equal to the sum of the third and fourth terms of equation (7), we obtain

$$\mathbf{s}(-3\mathbf{b}_1 + \mathbf{b}_2) = -4[\bar{1}10] + [001]. \tag{8}$$

Equation (8) corresponds to the step vector of the CSL-pattern from *I* to *F* in Fig. 4 where a lattice point *I* is the centre of the characteristic 3 × 3 cluster of CSL-points and *F* is the centre of the 3 × 3 cluster which will become CSL-points. We can find the same cluster at *G* if we shift crystal I by $-3\mathbf{b}_1 + \mathbf{b}_2$ from *F*. Since $-3\mathbf{b}_1$ comes from the SF in crystal I, the real step

vector $\mathbf{s}'$ results from adding a vector $-3\mathbf{b}_1$ to $\mathbf{s}(-3\mathbf{b}_1 + \mathbf{b}_2)$ of equation (8), then

$$\mathbf{s}' = \mathbf{s}(-3\mathbf{b}_1 + \mathbf{b}_2) - 3\mathbf{b}_1 = (-4 + \tfrac{1}{3})[\bar{1}10] + \tfrac{3}{4}[001]. \quad (9)$$

From equation (9) we have calculated that the shift vector of the boundary structure along the boundary plane is $(-4 + \frac{1}{3})$ $[\bar{1}10]$, and that the step height is $\frac{3}{4}[001]$. These two vectors are the same as those obtained from the structure image in Fig. 5.

For the $2H$ structure, the Burgers vector of a GBD was reported to be $\mathbf{b}_1$, and the step height to be $|001|_{2H}$ (Takata, Kitano & Komura, 1986). The basis vectors of the DSC-lattice and of the CSL as well as the step vectors of the CSL-pattern are also given in Table 1.

### References


ANTERROCHES, C. D' & BOURRET, A. (1984). *Philos. Mag.* A**49**, 783–807.

BOLLMANN, W. (1970). *Crystal Defects and Crystalline Interfaces.* Berlin: Springer.

FRIAUF, J. B. (1927*a*). *Phys. Rev.* **29**, 34–40.

FRIAUF, J. B. (1927*b*). *J. Am. Chem. Soc.* **49**, 3107–3114.

ICHINOSE, H. & ISHIDA, Y. (1981). *Philos. Mag.* A**43**, 1253–1264.

KING, A. H. & SMITH, D. A. (1980). *Acta Cryst.* A**36**, 335–343.

KITANO, Y., KOMURA, Y., KAJIWARA, H. & WATANABE, E. (1980). *Acta Cryst.* A**36**, 16–21.

KITANO, Y., TAKATA, M. & KOMURA, Y. (1986). *J. Microsc.* **142**, 181–189.

KITANO, Y., TAKATA, M. & KOMURA, Y. (1989). *J. Phys. (Paris).* In the press.

KOMURA, Y. (1962). *Acta Cryst.* **15**, 770–778.

LAVES, F. & WITTE, H. (1935). *Mettallwirtsch. Metallwiss. Metalltech.* **14**, 645–649.

POND, R. C. & BOLLMANN, W. (1979). *Philos. Trans. R. Soc. London Ser. A*, **292**, 449–472.

POND, R. C. & VLACHAVAS, D. S. (1983). *Proc. R. Soc. London Ser. A*, **386**, 95–143.

TAKATA, M., KITANO, Y. & KOMURA, Y. (1986). *Trans. Jpn Inst. Met.* **27**(Suppl.), 261–268.

TAKEDA, S. (1983). *J. Sci. Hiroshima Univ. Ser. A: Math. Phys. Chem.* **46**, 149–194.

TAKEDA, S., KITANO, Y. & KOMURA, Y. (1983). *J. Electron Microsc.* **32**, 105–114.


*Acta Cryst.* (1989). B**45**, 13–20

# Structure of $\mu$-$MnAl_4$ with Composition Close to that of Quasicrystal Phases


BY CLARA BRINK SHOEMAKER, DOUGLAS A. KESZLER AND DAVID P. SHOEMAKER

*Department of Chemistry, Oregon State University, Corvallis, Oregon* 97331, *USA*


(*Received* 10 *June* 1988; *accepted* 23 *August* 1988)


## Abstract

$MnAl_{4\cdot12}$, $M_r/100 = 32\cdot43$, $P6_3/mmc$, $a = 19\cdot98$ (1), $c = 24\cdot673$ (4) Å, $V = 8525$ (9) Å$^3$, atoms/cell = 563 (average), $D_x = 3\cdot556$ (2) g cm$^{-3}$, $\lambda$(Mo $K\alpha$) = 0·71069 Å, $\mu = 53\cdot05$ cm$^{-1}$, $F(000) = 8639$, $T =$ 296 K, final $R = 0\cdot053$ for 1397 reflections with $I > 2\sigma$. The structure is of interest with relation to quasicrystal phases in the Mn–Al system. Parts of the structure resemble that of $\varphi$-$Mn_3Al_{10}$. Neither complete Mackay icosahedra (MI), nor 105-atom Bergman clusters are present, but different fragments of MI occur. Most interstices are octahedral, tetrahedral, or trigonal prismatic. The Mn atoms have zero to two Mn atoms in the first coordination shell and four to twelve Mn atoms in the second shell. Of the Mn atoms 108 have icosahedral coordination, two have CN9. Of the 453 Al atoms 6·6% have icosahedral coordination, 35·8% are coordinated by a pentagonal prism of Al atoms with two Mn atoms at the poles, 26·5% have CN13, 25·6% have irregular CN12 arrangements formed by parts of icosahedra and pentagonal prisms, and the remaining 5·5% have other coordinations varying between 11 and 15. Two Al positions are partly occupied. The distance ranges are Mn–Mn 2·678–2·758, Mn–Al 2·359–2·874, Al–Al 2·527–3·166 Å (e.s.d. range: 0·002–0·014 Å). There are almost linear rows of atoms, which center icosahedra or pentagonal prisms. Approximate icosahedral symmetry is propagated in the direction of these rows.


## Introduction

A phase of assumed approximate composition $MnAl_6$, exhibiting non-crystallographic (icosahedral) symmetry in its electron diffraction pattern, was discovered by Shechtman, Blech, Gratias & Cahn (1984). This phase was formed by extremely rapid cooling from a melt. Subsequently, more non-equilibrium phases have been discovered that exhibit orientational symmetry, but lack periodicity in one or more dimensions; phases of this kind have been called quasicrystalline. Possibly, clues to the structure of a quasicrystalline phase may be provided by the structure of an equilibrium crystalline phase of similar composition. The crystal structure of

0108-7681/89/010013-08$03.00